Iraqi Journal of Biotechnology, May 2019, Vol. 18, No. 2, 201-215

Molecular and Nanotechnical Study for Antibiofilm Formation and *CsuE* Gene Expression Activities of Synthesized Iron Oxide Nanoparticles Against Multidrug-Resistant *Acinetobacter baumannii* Isolates

Haider Turky AL-Mousawi[1] , Mohammed I. AL-Taee[2] , Maarib N. Rasheed[2] , Qabas Nima AL-Hajjar[3]

[1]College of Biotechnology / University of Al-Qassim Green.
[2]Institute of Genetic Engineering and Biotechnology / University of Baghdad.
[3]Faculty of Pharmacy / University OF Kufa.

Received: February 27, 2019 / **Accepted:** April 7, 2019

Abstract: This study aimed to investigate the influence of synthesis of Iron Oxide Nanoparticles (Fe_3O_4NPs) by co-precipitation method on biofilm formation and *CsuE* gene expression in multidrug resistance *Acinetobacter baumannii* (MDR*A.b*) which represents one of the important causing agents of nosocomial infection. *A. baumannii* isolates used in current study and isolates from different clinical sources (wounds, burns, urine, sputum, blood and throat) that able to produce strong biofilm. Synthesis and characterisation the physical-chemical nature of Fe_3O_4 NPs was carried out using UV-visible spectrophotometer, fourier transform infrared (FT-IR), X-ray diffraction (XRD), Atomic force microscope (AFM) and scanning electron microscope (SEM). Results show that they were very fine crystalline sizes reaching to 11±1 nm by XRD ,with a mostly spherical in shape and average of nanoparticles size between (40- 47) nm by SEM and AFM, respectively. Minimum inhibitory concentration (MIC) and sub-MIC test of Fe_3O_4 NPs at concentrations (15.75 to 2000) µg/ml against *A.baumannii* isolates had been determined using tube broth method measured by optical densities values at 630 nm. The results of the experiment of the best sub-MIC with concentration of Fe_3O_4 NPs 125µg/ml showed a significant difference at $p>0.05$ the anti-biofilms inhibitory on polystyrene surface of microtiter plates for the bacteria isolate under study. Biofilm formation *CsuE* gene expression was investigated by using RT-qPCR technique with reference *16SrRNA* gene before and after treatment with Fe_3O_4 NPs. The results showed a significant difference at $p>0.05$ in Cycle threshold (Ct) values for *CsuE* gene expression of the isolates. The study concludes that the synthesized magnetic Fe_3O_4 NPs with 125µg/ml gave excellent antibiofilm activities and inhibitory efficiency against *A.baumannii* isolates and the potentiate to down regulate of gene expression fold for biofilm formation encoded by *CsuE* gene of *A.baumannii* leading as a result to have low biofilm production.

Keywords: MDR *Acinetobacter baumannii*, Iron Oxide Nanoparticles, Biofilm Formation, *CsuE* Biofilm gene and gene expression.

Corresponding author: (Email: haider.turky@yahoo.com).

Introduction:

Acinetobacter baumannii is one of the most challenging pathogens due to its particular multi-drug resistance (MDR) characteristics. World Health Organization (WHO) has recently selected *A.baumannii* as priority 1 (critical), highlighting its serious threats to public health (1).

A.baumannii is an opportunistic Gram negative bacterium, responsible for a broad range of nosocomial infections that frequently found in patients who are admitted to intensive care units (ICUs), ventilator-associated

pneumonia, UTI, meningitis, burn infection, wound sepsis and bloodstream infections, the mortality rates can reach 35% (2).

During the last two decades, *A.baumannii* has become a pathogen of increased clinical importance due to its remarkable ability to cause several hospital outbreaks of infections due to (MDR) however, it have been reported worldwide (3).

Biofilm is one of its important microbial virulence factors, however the ability of bacteria to form a biofilm and colonization of host tissue surfaces are an important step in the development of infection. It is the structural phenotype of microbial communities attached to the moist solid surfaces enclosed in the self-produced heterogeneous polymeric mixtures, as playing an important role in cell adhesion on biotic or abiotic and the interactions between cells that leads to increased morbidity and mortality(4).

The pathways are composed of several main parts, including bacteria populations, signal molecules, protein activators and target genes, which influence biofilm formation (5).

Early studies on the *A.baumannii* showed that pilus production mediated by the *Csu* usher-chaperone assembly system is required for the initial steps of bacterial attachment on abiotic surfaces, resulting in microcolony formation followed by the full development of biofilm (6).

The operon *CsuA/BABCDE* seems to be widespread among clinical isolates, the demonstrated ability of *A.baumannii* strain to adhere by pili to and to form biofilm on abiotic surfaces depending on the expression of *CsuE*, which is part of the *CsuA/BABCDE* usher-chaperone pili assembly system(7). The *CsuE* gene is highly preserved in *A.baumannii* and its absence from non-Acb complex species may explain why these species are not able to persist in the hospital environment (8).

Recently the use of nanotechnology to develop new biomaterials, they are displaying important applications in the field of medicine, which can manipulate suitably for desired applications include high sensitivity biomolecular diagnostics, antimicrobial-antibiofilm activities and therapeutics (magnetic target drug delivery, hyperthermia and magnetic resonance imaging) (9).

Nanoparticles usually ranging in dimension from 1-100 nanometers (nm), have properties unique from their bulk equivalent that related to the decrease in the dimensions of the materials to the atomic level (10).

Iron oxide nanoparticles (Fe_3O_4) appears to be more resist to microorganisms and are now widely used as antibacterial and antibiofilm agents due to their remarkable properties, superparamagnetism, size (about 10–20 nm) and possibility of receiving a biocompatible coating (11,12).

The ability of Iron oxide nanoparticles to block bacterial growth is represent in prevention of the glycocalyx formation that was helpful to inhibit bacterial adhesion and following biofilm formation on the medical devices (11).

Materials and Methods:

Bacterial Strains:

Ten strong biofilm formation *A. baumannii* clinical isolates was used in this study, as described and identified previously, these isolates were recovered from (Burns swab, Wounds

swab, Sputum swab, Urine, Blood and Throat swab). Routine growth and strain preservation was carried out in Luria-Bertani broth (LB) for expression experiments.

Synthesis of the Fe_3O_4 magnetic iron oxide nanoparticles:

The synthesis of Iron oxide nanoparticles (Fe_3O_4 NPs) were prepared by the co-precipitation method described by (13) with modification. Experimental chemicals materials used in this study were ferric chloride ($FeCl_3.6H_2O$), ferrous sulfate ($FeSO_4.7H_2O$), sodium hydrochloride (HCl) and sodium hydroxide (NaOH). All the materials used were analytical grade.

Characterization Measurements of Fe_3O_4NPs:

Structural and optical properties to diagnose Fe_3O_4 NPs have been investigated in this study by various devices were carried out of some measurements are the fallowing technique.

UV-Visible Absorption Spectroscopy:

Investigate the optical Absorbance spectra of the Fe_3O_4 NPs solution were measured by a double-beam UV-VIS spectrophotometer model (Shimadzu-1). The wavelength range was recorded within the spectral from (295-1100 nm) (14).

X-Ray Diffraction Spectrum (XRD):

X-Ray diffraction device type (XRD, 6000- Shimadzu X-ray Diffractmeter) measurements to investigate the crystal structure (crystal phases and to determine the crystallite size of phase of Fe_3O_4 NPs (15).

The grains size was calculated from the width of the XRD peaks, was used to determine the crystallite size using Scherer's equation (16):

$$D = k\lambda / \beta \cos\theta \quad .....(1)$$

Scanning Electron Microscopy (SEM):

Scanning Electron Microscope, type (Inspect S50. fei company Easy Probe Tescan (Netherlands) is generally used to characterize the morphology properties, microstructure of materials (such as crystal structure, particle shape and size) of Fe_3O_4 NPs (17).

Atomic Force Microscopy (AFM):

Atomic Force Spectroscopy system model (AFM, AA-3000, USA) was used to characterized the size, surface, roughness, granularity volume distribution and topography of Fe_3O_4 NPs (18).

Fourier Transform Infrared (FTIR) Spectroscopy:

Fourier transform infrared spectroscopy was recorded on (FTIR, 8000 Series, Shimadzu) was a useful to investigate the various functional groups present in Fe_3O_4 NPs (19). The spectral rang of iron oxide nanoparticles was record from wavelength range of numbers 400- 4000 cm^{-1}.

Determination of minimum inhibitory concentration (MIC) of Fe_3O_4 NPs by Tube Method (TM):

The MIC of Fe_3O_4 NPs were determined by a method recommended

in (20) with some modifications. Briefly: *A.baumannii* isolates was cultured in nutrient agar for overnight. The sterile tubes were used each tube contains 9 ml of bacterial suspension in trypticase soy broth (TSB) with 1% glucose approximate 1.5 $\times 10^8$ cfu/ml . Then take 1 ml from each of Fe_3O_4 NPs concentrations (15.75, 31.25, 62.5, 125, 250, 500, 1000 and 2000) µg/ml after introduced to the ultrasound bath apparatus to ensure that the nanoparticles did not agglomerate, was mixed with 9 ml of bacterial growth, then incubated aerobically in shaker incubator for 24 h at 37°C. The bacterial growth in each tube was measured with spectrophotometer by optical density at 630 nm wavelength. The mean values of inhibition were calculated from triple reading in each test. A broth tube with only bacteria isolates without iron oxides NPs was used as control. MIC was read as the lowest concentration of iron oxide nanoparticles at which there is tube without visible growth of the bacterial cells (21).

Effects of sub-MIC concentrations of Fe_3O_4 NPs on biofilm formation using Microtiter plate method (MTP):

The sub-MIC of Fe_3O_4 NPs were determined by a method recommended in (22) with some modifications. Briefly:

Overnight *A.baumannii* isolates culture was grown in brain heart infusion broth. Take 100 µl of bacterial suspension approximate 1.5 $\times 10^8$ cfu/ml was added to the sterile polystyrene microtiter plate with 96 well falt-bottom together with 100 µl of different concentration of Fe_3O_4 NPs, (125) µg/ml in each wells after introduced to the ultrasound bath apparatus to ensure that the nanoparticles did not agglomerate. The control wells contained 180 µl of brain heart infusion broth, and 20 µl of bacterial suspension. Then the culture plates were sealed with para film and were incubated aerobically for 24 h at 37°C. Then non attached bacterial cells were removed and washing the wells and three times with 200 µl of PBS (pH 7.2). After drying at room temperature, 200 µl of crystal violet (0.1%) added to the wells to stained the biofilms which remained adherent to the walls, then incubation for 10 min. The stained attached bacterial cells were rinsed three times with PBS (pH 7.2). Then plates were dried properly at room temperature then adding 200 µl of the destaining solution (95% ethanol) for 10 min. The controls were performed with crystal violet binding to the wells exposed only to the culture medium without bacteria. Then, the microtiter plate were measured the values of OD absorbance at 630 nm. Fe_3O_4 NPs effects on biofilm by values of optical density (OD) at 630 nm were determined using ELISA Reader (23). The inhibition of biofilm formation percentages of iron oxide nanoparticles for each bacterial isolates was calculated as formal described by (24).

Inhibition efficiency(%)=((Control OD-test OD)/(Control OD)) ×100% …… (2)

The microtiter plate antibiofilim assay estimates the percentage of bacterial biofilm reduction, in relative to the control wells, which were set at 100% to indicate the absence of Fe_3O_4 NPs. In contrast, negative percentage results indicate no inhibition activity of iron oxide nanoparticles on biofilm organization.

Nucleic acid RNA extraction and relative quantitative real-time PCR of *CsuE* gene:

Total RNA was extracted from isolated colonies for all *A.baumannii* isolates from different sources that gaving strong biofilm formation was done before treatment with the Fe_3O_4 NPs, extract with an DONGSHENG BIOTECH General RNA Extraction kit (Korea) according the manufacturer's recommendations steps. The RNA concentrations were determined by using NanoDrop Lite Spectrophotometer. Then The RNA was used as a template from which to synthesise cDNA. This standard protocol applies to a single reaction where only template, and water need to be added to the RT FDmix, and the programs used according the manufacturer's recommended. After the PCR program, the synthesis cDNA samples were separated by electrophoresis to shows the band intensity was quantified. Quantification of specific *CsuE* gene F 5′-TAG CGG GCC TGA TGG CAA TT-3′, R 5′-ACC CAG GGC TCT CAA AGA AG-3′ (184 bp) (25) and the reference gene *16SrRNA* F 5′- CAG CTC GTG TCG TGA GAT GT -3, R 5′- CGT AAG GGC CAT GAT GAC TT -3′ **(**150 bp) (26) was used as a control was performed using the real-time PCR in the CFX-96 Thermal Cycler (BioRad Laboratories, Hercules, CA, USA), by using WizOureTM qPCR Master (SYPER) 1-Step RT-qPCR System. This standard protocol applies to single reaction where only template primers, and water need to be added to the qPCR Master (SYPER) and ROD Dye, with the following cycle profile: Initial Denaturation 1 cycle at 95 °C for 5 min followed by 40 cycles at 95 °C for 15 s Denaturation and annealing at 57 °C for 1 min, finally Melting curve analysis 1 cycle at 95 °C for 5 s.

The data results of qRT-PCR calculate as it is a direct comparison of threshold cycles (Ct) values between for target and reference (housekeeping) genes were analyzed by the relative quantification gene expression levels (fold change) analysis and one melting curve cycle were analyzed and optimized the ΔΔCt method using software that described by (27). The PCR amplification as following equations:

ΔCt= Ct target – Ct reference gene…. (3)
ΔΔCt=(Ct target – Ct reference) sample - (Ct target – Ct reference) Calibrator .. (4)
Fold change = $2^{-\Delta\Delta CT}$ …….. (5)

So, the relative expression changes in mRNA expression levels were determined using comparative threshold cycle (CT) value method ($2^{-\Delta\Delta Ct}$**)** between the iron oxide nanoparticles treated and untreated for *A. baumannii* isolates.

After adding the Fe_3O_4 NPs on *CsuE* expression:

Relative quantitative real-time PCR (rqRT-PCR) was performed to compare the effect of iron oxide nanoparticles Fe_3O_4 NPs at appropriate concentration on *CsuE* expression gene. Briefly, Lauria Bertini broth tubes 1×10^8 CFU/mL of bacterial cells were inoculated into concentrations of (125) µg/ml of Fe_3O_4 NPs and incubated for 24 hrs at 37 °C. After that, RNA extraction was done by the same steps by DONGSHENG BIOTECH General RNA Extraction kit. Use same genes, RT master mix and programs that used before add Fe_3O_4 NPs, and compare the

number of isolates that overexpressed *CsuE* gene.

Statistical Analysis:

The results data were analyzed by using Statistical analysis system by using computer program (SPSS), analysis of variance (ANOVA) were used, the level of probability at P values below of ≤ 0.05 that used to identify a significant difference (28).

Results and Discussion:

Synthesis of Magnetic Iron Oxide Nanoparticles Fe_3O_4 NPs:

The result indicated successfully synthesizing of magnetic iron oxide nanoparticles Fe_3O_4 NPs and show a dark black color with ferromagnetic properties and agreement with (29) them synthesis iron oxide nanoparticles by chemical method.

Characterization of synthesized Fe_3O_4 NPs:

UV-Vis spectroscopy Assay:

The UV-Visible absorption spectrum were recorded in the wavelengths ranging region from (290 to 1100 nm) were examined to detect the property of the synthesized iron oxide nanoparticles prepared by precipitation method (Figure 1). The results showed that the a single peak of the iron oxide nanoparticles were centered exhibit strong surface plasmon resonance absorption below was recorded at approximately 402 nm, while the absorption edge lies between 312 and 750 nm, indicate the formation and the presence of Fe_3O_4 NPs. Various reports have established that the resonance peak of Fe_3O_4 NPs appears around this region, but the correct position depends on a numeral of factors such as particles size, and the surface adsorbed species (30).

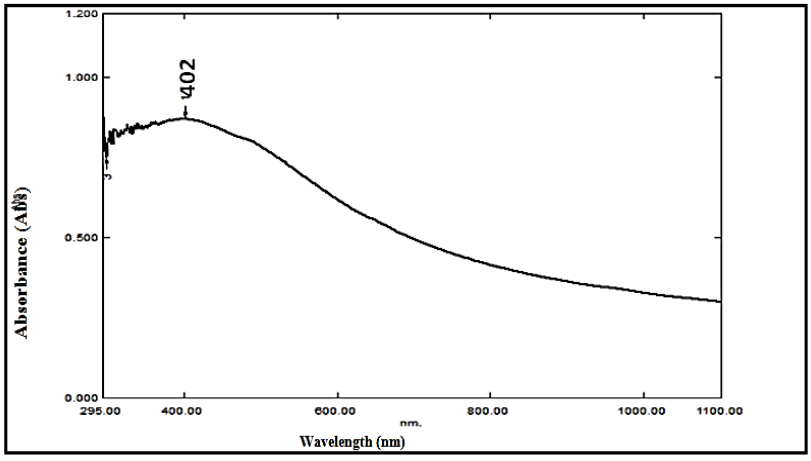

Figure (1): UV-Visible spectral analysis of synthesized iron oxide Nanoparticles (Fe_3O_4 NPs) recorded maximum absorbance at 402nm.

X-Ray diffraction Pattern Measurement (XRD):

The result of XRD it is found that there exist eight strong different diffraction peaks corresponding to the crystal planes of crystalline Fe_3O_4 NPs were observed at 2θ (θ=diffraction angle) values of 30.18°, 35.56°, 43.22°, 53.64°, 57.21°, 62.81°, 70.93° and

74.22°, corresponding to the crystalline distance (d) of (2.95), (2.52), (2.09), (1.70), (1.60), (1.47), (1.32) and (1.27) (Figure 2). Bragg reflection, of crystalline Fe_3O_4 NPs respectively. Indicating the black colored magnetic powders are magnetite nanoparticles with spinel phase structure of magnetite. The average crystallite size of the synthesized Fe_3O_4 NPs in present study can be estimated according to the Debye- Scherrer's equation was found to be in the range of (11±1) nm, which gives a correlation between particle size and peak broadening in XRD, that indicated the synthesis magnetic iron oxide nanoparticles is very fine. The Sharp peaks also suggest that the Fe_3O_4 NPs have good crystallinity and purity structure. Peak broadening observed is consistent with the small particle size(31).

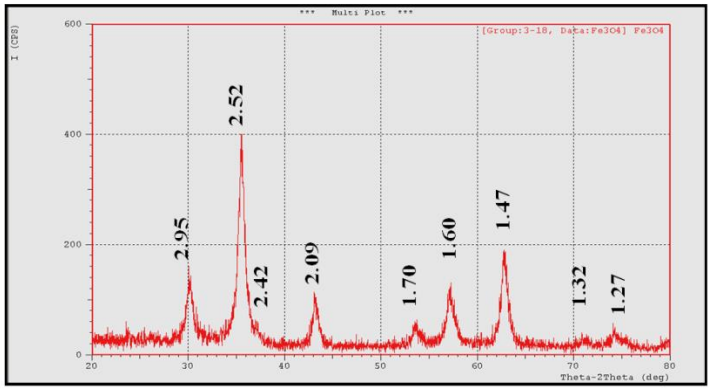

Figure (2): X-ray diffraction pattern of synthesized iron oxide Nanoparticles (Fe_3O_4 NPs).

Scanning Electron Microscope (FE-SEM):

SEM images it is evident that the sample consist of by a number quantity of the nanoparticles exhibit spherical shape Fe_3O_4 nanostructures. The average size of the obtained sample approximately 40 nm, indicating that homogeneous magnetite nanoparticles can be synthesized and rather good size distribution. The crystallites of magnetite particles are less agglomerated shown in (Figure 3).

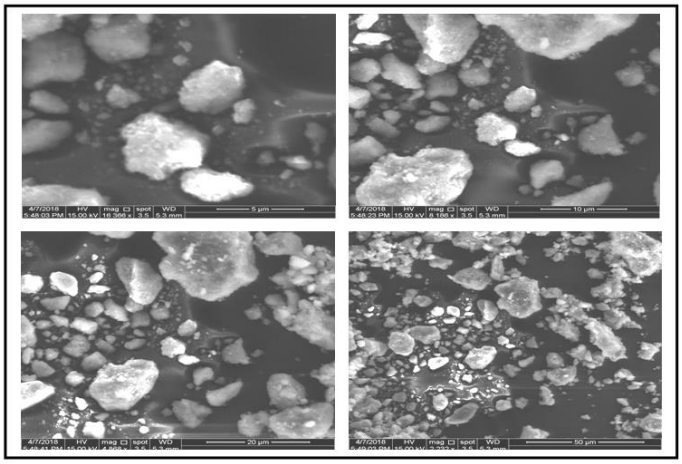

Figure (3): Scanning Electron Microscopy (SEM) images (5, 10, 20 and 50) μm of synthesized iron oxide Nanoparticles (Fe_3O_4 NPs).

Atomic Force Microscope (AFM) Analyses:

The images of AFM demonstrate an smart interaction among iron oxide nanoparticles leading to the formation of well discrete aggregates. (Figure 4 A, B) shows a three-dimensional (3D) and two-dimensional (2D) image of a section of the surface of the Fe_3O_4 NPs, where the high molecular clusters which is up 14.93 nm. The average of diameters and sizes composite of Fe_3O_4 NPs that demonstrate in numerous peaks, the highly peaks is (39) from (8-90) nm. Thus the rate of particles sizes (means of average particle size) of the Fe_3O_4 NPs is 47 nm that shown in (Figure 3-4 C). It is indicating that the Fe_3O_4 NPs synthesis is manufacturing infinitesimal and uniformly arranged. As the nanoparticles aggregates undergo a brownian action in suspension, scanning in liquid cannot be used for nanoparticle sizing. Sample preparation is vital in order to get useful AFM images. Samples must be thin enough and must hold fast well to the surface, otherwise the scanning method will producing artifacts (32).

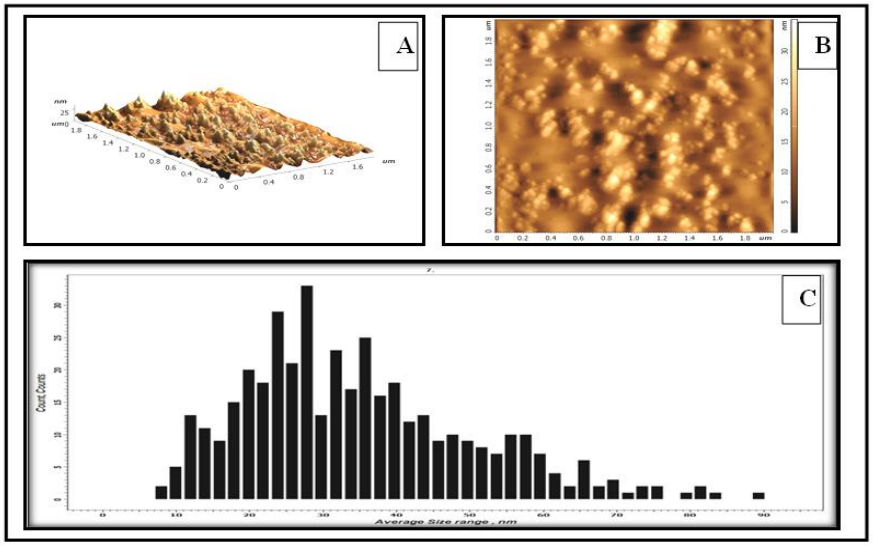

Figure (4): Granularity volume distribution chart Image of the synthesized iron oxide nanoparticles (Fe_3O_4 NPs) by Atomic Force Microscope topographic images (A) Three-Dimensional, (B) Two-Dimensional and (C) Average particle size.

Fourier Transform Infrared Spectrum (FTIR):

The results obtained by FTIR spectroscopy was presented in (Figure 5) shows the FTIR spectrum of Fe_3O_4 NPs prepared with absorption peaks located in the region of 4000 cm^{-1} to 400 cm^{-1}, by strong bands at (3415.70, 2362.64, 1633.59, 1433.01, 1008.70, 630.68, 580.53, 567.03 and 451.31) cm^{-1}, corresponds assigned to (hydroxyl group -OH-free, (CH) groups, carbonyl (–C=O) group, phenolic compounds, (COO-) stretching, (C-O) stretch and (C-H) stretching of phenyl ring).

The presence of magnetite iron oxide nanoparticles can be seen by three strong absorption bands at peaks 580.53, 567.03 and 451.31 cm^{-1}, which, corresponding to the Fe-O stretching band of bulk magnetite (Fe_3O_4). The

band locations and amounts of absorption peaks are dependent on chemical composition, crystalline structure and also on morphology (33).

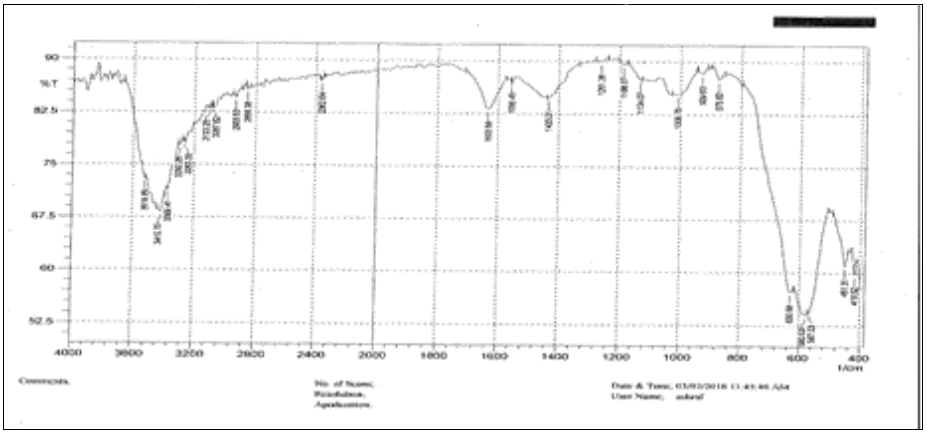

Figure (5): FTIR spectra pattern of dried powder of synthesized iron oxide Nanoparticles (Fe_3O_4 NPs)

Determination the Minimum Inhibitory Concentration (MIC) Test Results for Fe_3O_4 Nanoparticles:

The result MIC of Fe_3O_4 NPs for the antibacterial activities in Tube method was presented in (Figure 6), shows the optical density (OD) at 630 nm of the means for each concentrations of *A.baumannii* isolates under study, bacterial culture growth in the presence of Fe3O4 NPs by Tube broth medium method compare with (OD) of the control without NPs. The result showed that the a significant ($p<0.05$) between concentrations (15.75, 31.25, 62.5, 125, 250, 500, 1000 and 2000) µg /ml of synthesis Fe_3O_4 NPs that used are demonstrated different result, the lowest concentration give an inhibition the number of cells of 125 µg /ml concentration, therefore was the best-used concentration of Fe_3O_4 NPs for inhibiting growth of *A.baumannii* isolates.

The mode action of the Fe_3O_4 nanoparticles materials were interpreted in terms of the following series process: adsorption onto the bacterial cell surface, diffusion through the cell wall, binding to the cytoplasmic membrane and release of cytoplasmic constituent such as K+ ion, DNA, RNA, and death of the cell (34).

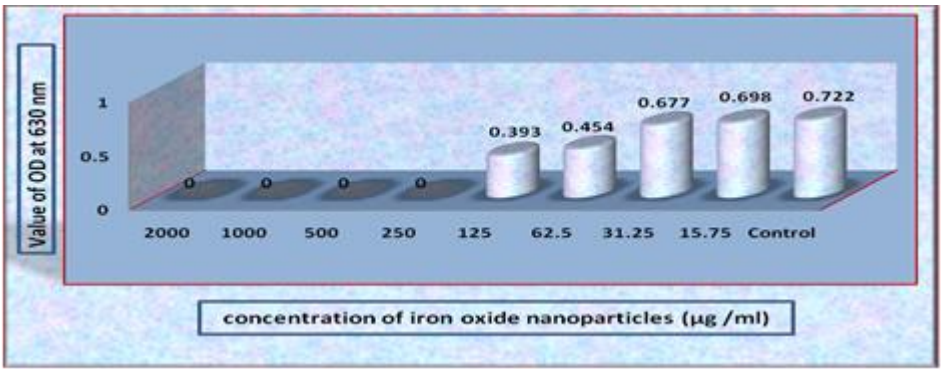

Figure (6): Effects of iron oxide Nanoparticles synthesized (Fe_3O_4 NPs) on values of OD at 630 nm of *A.baumannii.*

The Effect of sub-MIC of Fe_3O_4 NPs on Antibiofilm by Microtiter plate method:

The results showed that the sub-MIC of Fe_3O_4 NPs was 125 µg /ml concentration exhibited a significant reduction in biofilm growth against all *A.baumannii* isolates by the absorbance values was decreased for all isolates after a treatment with sub-MIC of these Fe_3O_4 NPs, with different thickness degrees the absorbance values compared with absorbance values of control that untreated with Fe_3O_4 NPs (Figure 7). These results indicated that there is a significant difference on biofilm formation after treatment with sub MIC of Fe_3O_4 NPs.

The sub-MIC of Fe_3O_4 NPs inhibited bacterial adhesion on polystyrene surface and consequently causes biofilms detachment and this causes decreased in absorbance values of biofilms (35).

Many studies have shown the size dependent antimicrobial and anti-biofilm effects of these nanoparticles and their physico-chemical properties. The small sizes of nanoparticles enables those to penetrate the biofilm matrix and have a high surface to volume ratio, which promotes effective interactions with bacteria and to make contact with bacterial cells cause inhibition of biofilm Furthermore the Fe3O4 NPs inhibited biofilm production by blocking the formation of exopolysachrides (36).

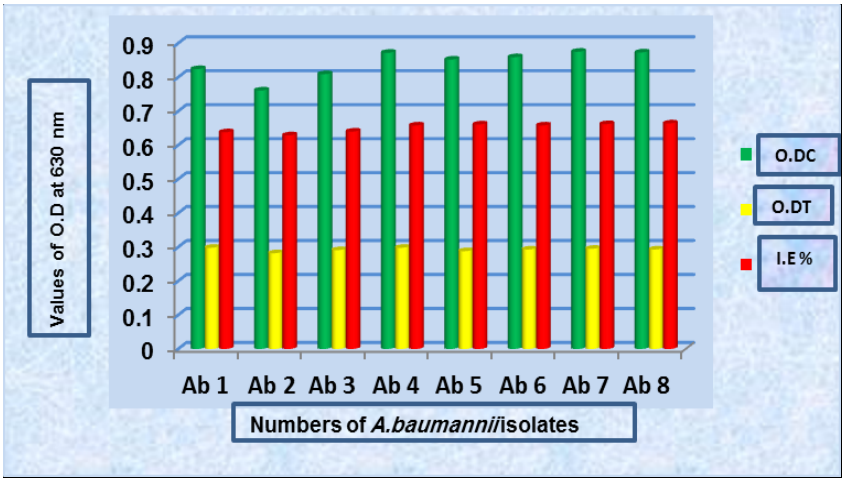

Figure (7): biofilm inhibition activity of synthesized iron oxide nanoparticles (Fe_3O_4 NPs) against *A.baumannii* isolates.

Gene expression analysis by using qRT PCR technique:

Total RNA and complementary DNA (cDNA) reverse transcription:

Before and after treatment with synthetic Fe_3O_4 NPs, total RNA was carefully extracted by using commercially available RNA extraction for *A.baumannii* isolates. The concentration of total RNA samples 260/280 ratios should be ranged between from (80 to 220) ng/ µl. The quality and purity of total RNA samples ranged between from (1.79 to 2.19)

ng/µl, this was measured using Nanodrop ND-2000 spectrophotometer. cDNA reverse transcription was conducted in the same day of RNA extraction, the efficiency of synthesized cDNA concentration was evaluated through gel electrophoresis to identified cDNA band before real time application (Figure 8).

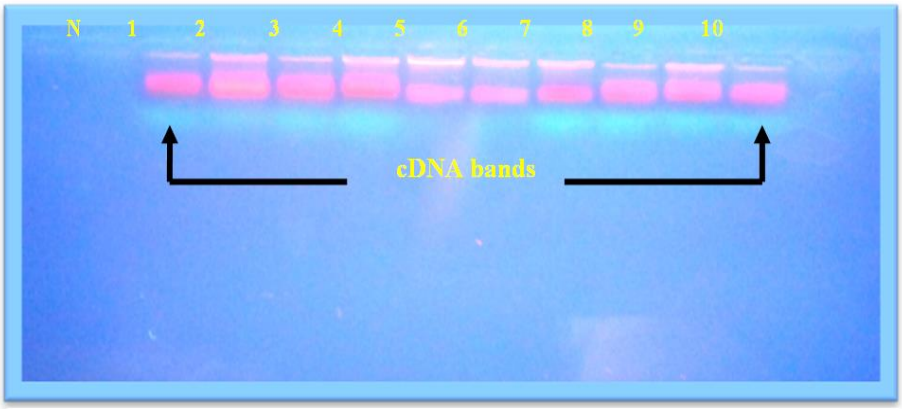

Figure (8): Gel electrophoresis detected cDNA bands from *A.baumannii* isolates (1% agarose,75V, for 30 min stained with ethidium bromide). Lane 1-10: cDNA. Lane N: Negative control (water).

Real time PCR quantification of *CsuE* gene Expression:

In the present study, quantitative RT-PCR assay analyzed the mRNA expression of *CsuE* gene showed significant variation in gene expression biofilm formation for *A.baumannii* isolates. The cycle threshold Ct values of *CsuE* gene amplification were recorded from the software of qRT-PCR, the statistical analysis shown significant differences at values $P<0.05$ the range from (14.16 to 22.13) before treatment with synthesized Fe_3O_4 NPs.

The pattern of amplification of the gene shown in (Figures 9 A and B) respectively, these variation submit to differences of the sources of isolates. After treatment with Fe_3O_4 NPs by using the concentration below the dose of sub MIC for each sample, the range of Ct value for *CsuE* gene from (17.02 to 24.20), there were significant difference according to LSD values at $P<0.05$ was found between isolates, the pattern of amplification of this gene showed in (Figures 9 C and D). The melting curve that show in Figures generated at the end of the PCR reaction show that all amplicon of the *CsuE* gene, this result indicates that no primer–dimmers were formed during the reactions.

The statistical analysis also appeared significant differences at values $P<0.05$ in Ct value where comparing between treated and untreated with Fe_3O_4 NPs for each isolates. Expression of the *CsuE* gene was decreased in all isolates that treated with Fe_3O_4 NPs, the latter has Ct values were highest than Ct values in untreated, this means decrease gene expression with the increased of Ct values.

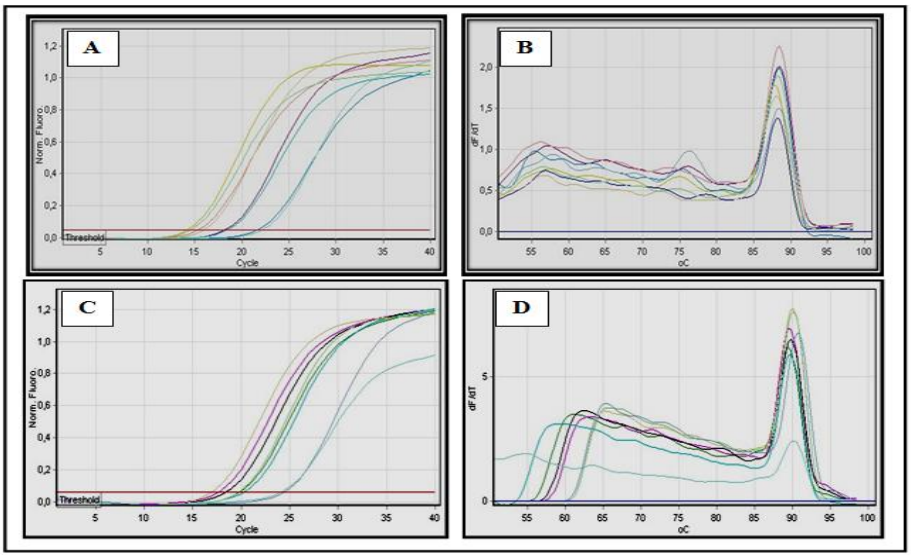

Figure (9): The amplification plots and Melting temperature curve ranged from 85°C to 90°C of *CsuE* gene before and after treatment with synthesis iron oxide nanoparticles (Fe_3O_4 NPs).

Real time PCR quantification of *16SrRNA* gene Expression:

In the present study *16SrRNA* is the (reference or internal control) gene was used. The range of Ct value of this gene in untreated with the synthesized iron oxide nanoparticles Fe_3O_4 NPs from (14.25 to 14.83) in all *A.baumannii* isolates, were we then treated with synthesis Fe_3O_4 NPs, the Ct value found not changing at high rang from (14.38 to 14.97). The statistical analysis shown non-significant difference was found in between of them isolates and between off before and after treatment, The pattern of amplification of the gene shown in (Figures 10 A and B) respectively. The purpose of the reference gene is to normalize the PCRs for the amount of RNA added to the reverse transcription reactions. Standard housekeeping genes usually are sufficient as internal control genes (37).

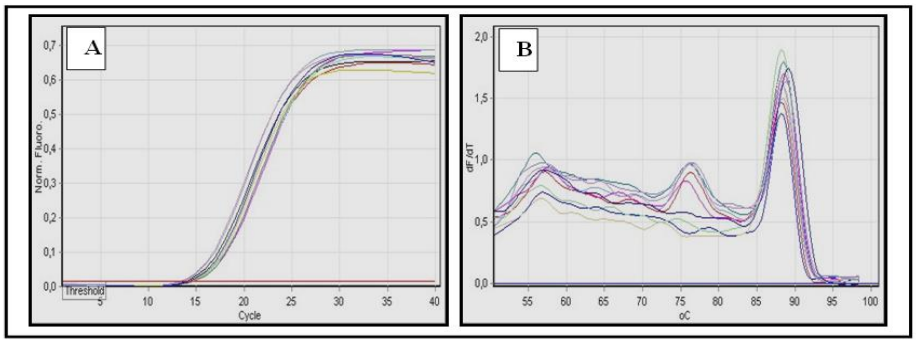

Figure (10): The amplification plots and Melting temperature curve ranged from 85°C to 90°C of housekeeping gene *16SrRNA*.

To determine whether *CsuE* expression is actually regulated, we performed qRT-PCR. Indeed biofilm formation in isolates with *CsuE* before treated with synthesized Fe_3O_4 NPs was significantly greater than after treated with synthesis nanoparticles ($p \leq 0.05$).

In the current study, quantitative RT-PCR evaluate analyzed the mRNA expression of *CsuE* and internal control

16SrRNA genes by comparing before and after treatment with synthesized Fe_3O_4 NPs for each isolate, The calculation of gene expression fold change was done by using relative quantification from delta delta Ct value (ΔΔCt) (37). This depends on normalization of Ct values calculating the ΔCt which is the difference between the mean Ct values of replica of *CsuE* cDNA amplification of each single case and that of the *16SrRNA*.

The alterations in gene expression levels can be visualized in (Table 1), which was generated using the data-analysis tools. These Table shows the mean of ΔCt (normalization Ct values) of each isolates for *CsuE* gene, depending on evaluate values for Ct of target genes with Ct for internal control. The results of ΔCT, ΔΔCT and $2^{-\Delta\Delta Ct}$ showed that there was a significant difference ($P<0.05$) in the values between the different studied isolates, this difference according to the source of isolated.

To calculate the folds of gene expression of *CsuE* gene in relation to the housekeeping gene. Genes that showed statistically significant for the result of $2^{-\Delta\Delta Ct}$ values for the isolates ranged determined from (0.059 to 0.279) for *CsuE* gene. These results indicate a significantly decrease expression of biofilm formation after treated with Fe_3O_4 NPs that shown in these Table. These results are consistent given that treated with Fe_3O_4 NPs causes the growth rate of the bacteria to decrease and decrease genes expressed.
The RT-PCR gene expression study indicated that a number of the genes within the bacterium were up-regulated at physiological biofilm. The importance of the *CsuE* gene in *A.baumannii* biofilm formation has been well established (6). Several previous researchers from studies about this bacterium and correlation with adherence and biofilm formation. Variation in the expression of factors involved in these pathways may account for the different capacity of bacterial strains to form biofilms and therefore to colonize or infect the host environment (38).

Table (1): Fold of gene expression of *CsuE* gene depending on ΔΔCt method.

No. of isolates	Treatment	Ct *CsuE* of Target gene	Ct of reference *16SrRNA*	ΔCt Target (Ct *CsuE* - Ct internal control	ΔΔCt	$2^{-\Delta\Delta Ct}$ Fold of gene expression
Ab 1	Untreated	14.56	14.83	- 0.27	3.01	0.124
	Treated	17.70	14.96	2.74		
Ab 2	Untreated	15.54	14.72	0.87	4.08	0.059
	Treated	19.90	14.95	4.95		
Ab 3	Untreated	14.39	14.28	0.11	3.84	0.069
	Treated	18.53	14.58	3.95		
Ab 4	Untreated	15.93	14.61	1.35	3.47	0.090
	Treated	19.77	14.95	4.82		
Ab 5	Untreated	14.16	14.25	-0.09	2.45	0.183
	Treated	17.02	14.66	2.36		
Ab 5	Untreated	21.62	14.44	7.18	2.37	0.193
	Treated	24.20	14.65	9.55		
Ab 7	Untreated	22.13	14.81	7.32	2.22	0.214
	Treated	24.51	14.97	9.54		
Ab 8	Untreated	18.24	14.45	3.79	1.84	0.279
	Treated	20.30	14.67	5.63		
LSD value (P-value)		---	---	---	---	**0.117 * (0.044)**
*** (P<0.05).**						

Reference:

1. WHO. and Geneva. (2017). WHO Publishes List of Bacteria for which New Antibiotics are Urgently Needed.
2. Antunes, L.C.S.; Visca, P. and Towner, K. J. (2014). *Acinetobacter baumannii*: evolution of a global pathogen. *Pathogens and Disease*, 71(3): 292-301.
3. Maj, F.M.L.; O'conor, D.K.; USMA, C.; Joseph, C. B. and Usma, C. (2017). Evaluation of Virulence Gene Expression Patterns in *Acinetobacter baumannii* Using Quantitative Real-Time Polymerase Chain Reaction Array. *Military Medicine*, 181.
4. Lee, J.; Kim, Y.; Ryu, S.Y.; Cho, M.H. and Lee, J. (2014). Resveratrol oligomers inhibit biofilm formation of *Escherichia coli* 0157: H7 and *Pseudomonas aeruginosa*. *J. Nat. Prod*., 77(1): 168-172.
5. Moghadam, S. O.; Pourmand, M.R. and Aminharati, F. (2014). Biofilm formation and antimicrobial resistance in methicillin -resistant *Staphylococcus aureus* isolated from burn patients, Iran. *J. Infect. Dev. Ctries*, 8(12):1511-1517.
6. Thomas, L.; Russell, A. D. and Maillard, J. Y. (2008). Antimicrobial activity of chlorhexidine diacetate and benzalkonium chloride against *Pseudomonas aeruginosa* and its response to biocide residues. *Journal of applied microbiology*, 98: 533-543.
7. Breij, D.A.D.L.; Lagendijk, E.; Meer, V.R.; Koster, J.; Bloemberg, A.G.; Woterbeek, R., *et al*. (2010). Do biofilm formation and interactions with human cells explain the clinical success of *Acinetobacter baumannii*. *PloS One*, 5: 107-132.
8. Sahl, J.W.; John, D. G.; Schupp, J. M.; Victor, G.; Waddell, V. G; Driebe, E.M., *et al*. (2013). Evolution of a Pathogen: A Comparative Genomics Analysis Identifies a Genetic Pathway to Pathogenesis in *Acinetobacter*. *PLOS*.
9. Ramasamy, M. and Lee, J. (2016). Recent nanotechnology approaches for prevention and treatment of bioflm-associated infections on medical devices. *BioMed Research International*, 1: 1-17.
10. Boisseau, P. and Loubaton, B. (2011). Nanomedicine, nanotechnology in medicine. *Comptes. Rendus. Physique*., 12: 620-636.
11. Ansari, M. A.; Khan, H. M.; Khan, A. A.; Cameotra, S. S. and Alzohairy, M. A. (2015). Anti-biofilm efficacy of silver nanoparticles against MRSA and MRSE isolated from wounds in a tertiary care hospital. *Indian Journal of Medical Microbiology*, 33: 101–109.
12. Arias, Y.F.; Gabriela, V.; Raul, O.; Ulises, A.; Souad, A. and Raul, V. (2018). Magnetic phase transitions in ferrite nanoparticles characterized by electron spin resonance. *Journal of Applied Physics* 117: 17A503.
13. Wang, B.; Wei, Q. and Qu, S. (2013). Synthesis and characterization of uniform and crystalline magnetite nanoparticles via oxidation-precipitation and modified co-precipitation methods. *Int. J. Electrochem. Sci*., 8: 3786-3793.
14. Meshram, L.; Rakesh, K.P.; Khare, M.; Bagde, S.; Sahare, N.K. and Singh, V. (2012).Comparative analysis between biofilm formation of commensal and pathogenic *Escherichia coli* isolate. *Asiatic Journal of Biotechnology Resources*, 3(10): 1441-1446.
15. Tsuji, K.; Nakano, K.; Takahashi, Y.; Hayashi, K. and Ro, C.U. (2012). X-ray. *The Journal of Infectious Diseases*, 215, (supp l-1) 15: S52–S57.
16. Cullity B.D and Stock S.R. (2001). Elements of x-ray diffraction, Pearson education, 3rd edition, published by Prentice Hall, 558.
17. Hall, J.P.; dobrovolskaia, M.A.; Patri, A.K. and MaNeil, S.E. (2007). Characterization of nanoparticles for therapeutic. Nanomedicine (London).
18. Magonov, S.N.; Elings, V. and Whangbo, M.H. (2013). Phase imaging and stiffness in tapping-mode atomic force microscopy. *Surf. Sci*., 375: 385–391.
19. Soares, J. (2014). Optical materials characterization Advanced Materials Spectrometry. *Analytical Chemistry*. 84: 636–668.
20. (CLSI), Clinical and Laboratory Standards Institute. (2013). Performance Standards for Antimicrobial Susceptibility Testing; Twenty-Third Informational Supplement. 33(1): M100-S23.
21. Chao, W.; Nan, S.; Zan-Zan, Z.; Yang-Long, H.; Venkatramana, S.S. and Chuan, X.Z. (2012). Magnetic iron oxide nanoparticles: Synthesis and surface

coating techniques for biomedical applications. *Chin. Phys. B*., 23(3): 037-503.
22. Idalina, M.; Graça, J.; Lopes, H.; Lopes, S. and Pereira, M.O. (2013). Antimicrobial Pressure of Ciprofloxacin and Gentamicin on Biofilm Development by an Endoscope-Isolated *Pseudomonas aeruginosa*. *J. Biotechnology, Article ID 178646*, 10.
23. Gitanjali, K.B. and Dhananjay, K. (2015). Biofilm Producing Multidrug Resistant *Acinetobacter baumannii*: An Emerging Challenge. *Journal of Clinical and Diagnostic Research*, 9(1): DC08-DC10.
24. Namasivayam, S.K.R.; Preethi, M.; Bharani, A.R.S.; Robin, G. and Latha, B. (2013). Biofilm Inhibitory Effect of Nanoparticles coated catheter against *Staphylococcus aureus* and Evaluation of its Synergistic Effects with Antibiotics. *Inte. J. Bio. Pharm. Res*., 3: 259-265.
25. Skurikhina, Y.U.; Ibragimova, T.D.; Skurikhina, L.A. and Turkutyukov, V.B. (2016). Molecular Epidemiological Analysis of *Acinetobacter baumannii* Strains Isolated in Patients with Burn Injury. *Clinical medicine, CTM* (8)1.
26. Higgins, P.G.; Wisplinghoff, H.; Stefanik D. and Seifert. H. (2004). Selection of topisomerase mutations and overexpresson of adeB mRNA transcripts during an outbreak of *Acinetobacter baumannii*. *J. Antimicrob. Chemother*., 54: 821-823.
27. Schmittgen, T.D.; Lee, E.J.; Jiang, J.; Sarkar, A.; Yang, L.; Elton, T.S., *et al*. (2008). Real-time PCR quantification of precursor and mature microRNA. *Methods*, 44: 31-8.
28. Urdan, T.C. (2005). Statistics In Plain English, 2nd ed. Lawrence Erlbaum Associates, London : 130-143.
29. El-Sigeny, S.M. and Abou Taleb, M.F. (2015). Synthesis, Characterization, and Application of Dendrimer Modified Magnetite Nanoparticles as Antimicrobial Agent. *Life Science Journal*, 12(6).
30. Pal, S.; Tak, Y.K. and Song, J.M. (2007). Does the antibacterial activity of silver nanoparticles depend on the shape of the nanoparticle? A study of the Gram-negative bacterium *Escherichia coli*. *Applied and Environmental Microbiology*, 73: 1712–1720.
31. Zhang, Y.; Dasari, S. T. P.; Deng, H. and Yu, H. (2015). Antimicrobial Activity of Gold Nanoparticles and Ionic Gold. *J. Environ Sci. Health C Environ Carcinog Ecotoxicol Rev*., 33(3): 286-327.
32. Inderam D.C.E.I. and Certu, C.M. (2012). Assesing Fe3O4 nanoparticle size by DLS, XRD and AFM. *Journal of optoelectronics and advanced materials*, 14(5- 6): 460 – 466.
33. Balamurughan, M.G.; Mohanraj, S.; Kodhaiyolii, S. and Pugalenthi, V. (2014). Ocimum sanctum leaf extract mediated green synthesis of iron oxide nanoparticles: spectroscopic and microscopic studies. *J. of Chemical and Pharmaceutical Sci*, 4: 201-204.
34. Nayamadi A.M.; Kompany, A. and Mashreghi, M. (2018). Characterization, antibacterial and cytotoxicity studies of graphene-Fe3O4 nanocomposites and Fe3O4 nanoparticles synthesized by a facile solvothermal method. *Materials Chemistry and Physics*, 213(1): 285-294.
35. Parsek, M.R. and Singh, P.K. (2003). Bacterial biofilms: an emerging link to disease pathogenesis. *Annu. Rev. Microbiol*., 57:677-701.
36. Sharmal, P.; Rana, S.; Barick, K.C.; Kumar, C.S.; alunke, H.G. and Hassan, P.A. (2015). Biocompatible phosphate anchored Fe3O4 nanocarriers for drug delivery and hyperthermia. *New J. Chem*., 5500-5508.
37. Schmittgen, T.D.; Lee, E.J.; Jiang, J.; Sarkar, A.; Yang L.; Elton, T.S. *et al*. (2008). Real-time PCR quantification of precursor and mature microRNA. *Methods*, 44: 31-8.
38. Bahador, A.; Farshadzadeh, Z.; Mokhtaran, R. and Hashemi, F.B. (2018). Association of virulence gene expression with colistin-resistance in *Acinetobacter baumannii*: analysis of genotype, antimicrobial susceptibility, and biofilm formation. *Annals of Clinical Microbiology and Antimicrobials*, 17:24.